



Prognostic value of tumor solid-part size and solid-part volume in patients with clinical stage I non-small cell lung cancer

Yoshihisa Shimada¹, Hideyuki Furumoto¹, Kentaro Imai¹, Ryuhei Masuno², Jun Matsubayashi³, Naohiro Kajiwara¹, Tatsuo Ohira¹, Norihiko Ikeda¹

¹Department of Thoracic Surgery, ²Department of Radiology, ³Department of Anatomic Pathology, Tokyo Medical University, Tokyo, Japan

Contributions: (I) Conception and design: Y Shimada; (II) Administrative support: N Ikeda; (III) Provision of study materials or patients: Y Shimada, H Furumoto, K Imai, R Masuno, J Matsubayashi; (IV) Collection and assembly of data: Y Shimada, H Furumoto, K Imai; (V) Data analysis and interpretation: Y Shimada; (VI) Manuscript writing: All authors; (VII) Final approval of manuscript: All authors.

Correspondence to: Yoshihisa Shimada, MD, PhD. Department of Thoracic Surgery, Tokyo Medical University, 6-7-1 Nishishinjuku, Shinjuku-ku, Tokyo 160-0023, Japan. Email: zenkyu@za3.so-net.ne.jp.

Background: This study aimed to predict the malignant potential of clinical stage I non-small cell lung cancer (c-I NSCLC) by semiautomatic three-dimensional (3D) volumetric measurement of a tumor (3D-data) and the axial computed tomography (CT) data derived from a 3D volumetric dataset (2D-data). The predictive performance was evaluated in terms of overall survival (OS), disease-free survival (DFS), and pathological invasive factors (positive lymphatic invasion, blood vessel invasion, pleural invasion, or lymph node metastasis).

Methods: We identified 252 patients (122 male; mean age, 68 years; range, 23–84 years) with c-I NSCLC who underwent high resolution CT and reconstruction of 3D imaging, followed by complete resection between January 2012 and December 2015. In this study, 2D-data including whole tumor size (WTS) and solid-part size (SPS) and 3D-data including whole tumor volume (WTV) and solid-part volume (SPV) acquired by a 3D volume rendering software were analyzed.

Results: The area under the receiver operating characteristic (ROC) curve for WTS, SPS, WTV, SPV relevant to recurrence was 0.667, 0.727, 0.654, and 0.751 while analyses of ROC curves revealed optimal WTS, SPS, WTV, and SPV cut-off values to predict recurrence of 2.48 cm, 2.03 cm, 3,258 mm³ and 1,889 mm³, respectively. The association between SPS and SPV was the coefficient of determination (R^2) = 0.59. Multivariate analysis showed that SPV >1,889 mm³ (P=0.016) and male (P=0.041) were significant predictors of OS whereas SPV >1,889 mm³ (P=0.001), male (P=0.003), and the serum carcinoembryonic antigen value (P=0.041) were significantly correlated with DFS. SPS, SPV as well as the combination of SPS and SPV were all significantly correlated with the prediction of OS and DFS, and the incidence of pathological invasive factors.

Conclusions: SPV and the integrated use of SPS and SPV was highly beneficial for the prediction of postoperative prognosis in c-I NSCLC.

Keywords: Non-small cell lung cancer (NSCLC); volume; solid-part; three-dimensional CT (3DCT); stage I

Submitted Mar 09, 2018. Accepted for publication Oct 11, 2018.

doi: 10.21037/jtd.2018.11.08

View this article at: <http://dx.doi.org/10.21037/jtd.2018.11.08>

Introduction

Recent advances in imaging technology in the field of lung cancer have enabled the stratification of peripheral non-small cell lung cancer (NSCLC) patients according to their

prognosis by evaluating the high-resolution computed tomography (HRCT) features of their lung tumor (1-5). The ratio of the maximum consolidation diameter to the maximum tumor diameter is widely accepted for predicting

the outcome of patients who underwent not only pulmonary resection but also stereotactic body radiotherapy (4,6). Patients with a smaller proportion of solid-part size in lung cancer on HRCT had a significantly lower recurrence rate regardless of the operative procedures, suggesting that the separate measurements of the solid-part size and the whole tumor size are highly beneficial for tailored treatment planning (2,4). Although decreased CT-measured solid-part size of lung cancer, especially adenocarcinoma, is reported to be a better prognostic factor, small lung lesions with an irregularly shaped solid part in the greatest dimension are often encountered and can cause intraobserver and interobserver variability in practice.

To address the issue, we preoperatively take advantage of three-dimensional (3D) visualization using volume rendered imaging technique (3D-VRT) not only for surgical simulation but also for possible prediction of the pathobiological features of a lung tumor and prognostic outcomes by conducting volumetric quantification of the solid and non-solid parts separately using a 3DCT workstation (Fujifilm Synapse Vincent system; Fujifilm Corp., Tokyo, Japan) (7-11). Semiautomatic volumetric measurement of a tumor presents a pixel-wise segmentation of the 3DCT volume depending on the attenuation of each single voxel. As the calculation of the solid-part and non-solid-part volume based on 3D-VRT is consistent, the volumetric quantification is more likely to reflect the patient's prognosis.

This study aimed to investigate the clinical outcomes and pathological malignant grade of patients with resected clinical stage I NSCLC by comparing preoperative HRCT and 3D-VRT oriented radiologic parameters such as solid-part size and solid-part volume.

Methods

Patients

We identified 252 patients with clinical stage I NSCLC who underwent complete resection between January 2012 and December 2015 at our department. HRCT and 3DCT were preoperatively performed for all patients using the Fujifilm Synapse Vincent system. The Tumor Node Metastasis (TNM) stage was determined in accordance with the 8th edition of the TNM classification of malignant tumors (12). Preoperative evaluation included physical examination, chest radiography, chest and abdomen CT, blood examination, and F-18 fluorodeoxyglucose-positron

emission tomography/computed tomography (FDG-PET/CT). The protocols for data collection and analysis were approved and the need to obtain written informed consent from each patient was waived by the Institutional Review Board of Tokyo Medical University.

HRCT and 3DCT evaluation for primary tumors

The patients underwent contrast-enhanced CT imaging using a 64-channel multidetector CT system (Light Speed VCT, GE Medical systems, Milwaukee, WI, USA). Axial sections (1.25 mm in thickness) of the whole lung were reconstructed at intervals of 1.0 mm, and images were viewed on standard lung windows (level, -600 HU; width 1,500 HU) with the sharp kernel of the version "LUNG" and mediastinal windows (level, 30 HU; width 400 HU). Each CT image was acquired within 1 breath hold of about 5 s, after a delay of 70 s during which the contrast media injection took effect.

HRCT scans were evaluated by at least 2 surgeons (Y Shimada, H Furumoto, K Imai) and 1 radiologist (R Masuno) in consensus. We defined the solid-part size as the maximum dimension of the solid component of the lung windows excluding non-solid-part and measured the maximum diameter of tumor on axial CT slices (*Figure 1*). Non-solid-part representing ground glass opacity was defined as a misty increase in lung attenuation that did not obscure the underlying vascular markings.

The presented CT scan protocol has been used for both standard staging for lung cancer patients amenable to contrast radiography and 3D image conversion using the Synapse Vincent system. After digital imaging and communication in medicine data were transferred to a workstation using the indicated software, 3D-VRT were performed (*Figure 1*). In terms of volumetric measurement of a lung tumor, a density level of -300 HU is the threshold level that separate solid-part from non-solid-part by the software algorithm. This 3D tumor analysis provided the whole tumor volume, solid-part volume, and non-solid-part volume separately. The semiautomated volumetric analysis performed by the software needed to be adjusted manually. The results were confirmed in consensus (2 or 3 surgeons, Y Shimada, H Furumoto, K Imai, 1 radiologist, R Masuno).

Definition of pathological invasive factors and patient outcomes

The available pathology reports for all the 252 surgical

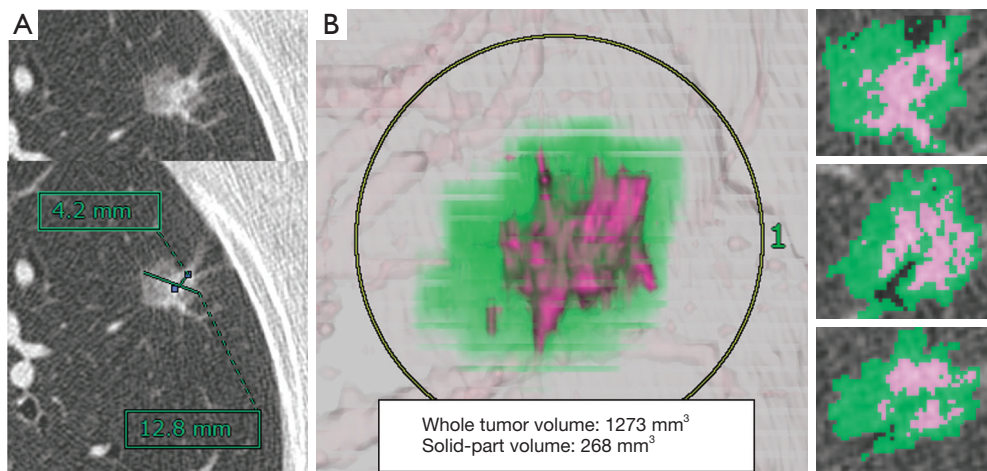


Figure 1 Representative comparative images of a lesion's whole tumor size and solid-part size on high-resolution computed tomography (HRCT), and whole tumor volume and solid-part volume measured by the Synapse Vincent system. An HRCT image presenting whole tumor size of 1.28 cm and solid-part size of 0.42 cm (A), and a three-dimensional (3D) volume rendered images of a tumor presenting whole tumor volume of 1,273 mm³ and solid-part volume of 268 mm³ with serial sections of the display (B). The 3D volume rendered images result in the detection of a solid-part with red and a ground glass opacity part with green.

specimens were reviewed in this study. Blood vessel invasion (V) was identified by the presence of erythrocytes in the lumen or an endothelial cell lining, or the presence of elastic tissue around large vessels while lymphatic invasion (Ly) was determined to be present when tumor cells floating in lymphatic vessels with no supporting smooth muscles or elastic fibers were identified. Resected lymph nodes were sectioned thicker than 2 mm and correctly embedded to ensure that the pathologists can identify all macro-metastases. At least single or 2 sections from blocks were prepared for diagnosis. Pathological invasive factors were defined as positive Ly, V, pleural invasion (PL), or lymph node metastasis. Overall survival (OS) was measured from the date of surgery to the date of death from any cause or the date on which the patients were last known to be alive. Disease-free survival (DFS) was measured from the date of surgery until the first event (relapse or death from any cause or the last follow-up visit).

Statistical analysis

The receiver operating characteristic (ROC) curves of each parameter were used to predict recurrence. The area under the ROC curve (AUC) with its 95% confidence interval (CI) was measured. OS and DFS curves were plotted using the Kaplan-Meier method, and differences in variables were determined using the log-rank test. Categorical

comparison was performed using the Pearson chi-squared test for discrete data and Student *t*-test for continuous data. Pearson correlation coefficient was used to determine the correlation between solid-part size and solid-part volume and the value of the coefficient of determination (R^2) was also provided. HRCT and 3DCT parameters measured by three observers were recorded, and interobserver variability by using a random sample of 100 patients was calculated for intraclass correlation coefficient (ICC). Univariate analysis for OS and DFS was performed using the Cox proportional hazards regression model whereas multivariate analysis was conducted with a stepwise variable selection for the Cox model. All tests were two-sided, and P values of less than 0.05 were considered to indicate a statistically significant difference. SPSS statistical software package (version 24.0; DDR3 RDIMM, SPSS Inc., Chicago, IL, USA) was used for statistical analysis.

Results

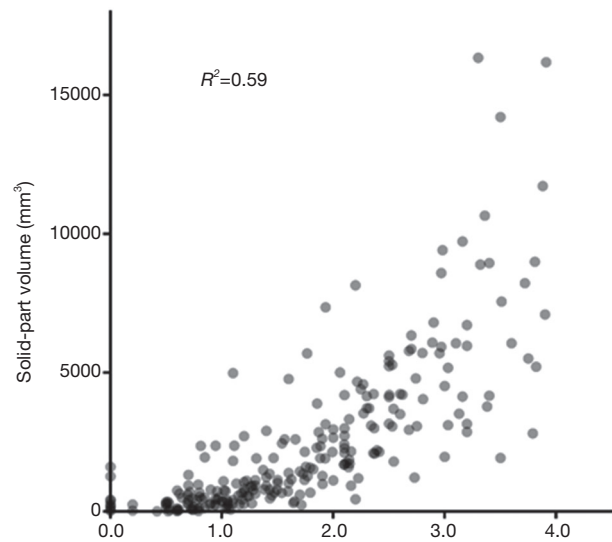
The characteristics of the patients were shown in *Table 1*. The median follow-up time for survivors was 1,233 days (range, 16 to 2,227 days). During the study period, recurrences occurred in 29 patients (12%), some of whom eventually died from these relapses (n=12, 5%). Only 1 patient died from subarachnoid hemorrhage during the study period. The clinical TNM stage showed 186 patients

Table 1 Patient characteristics

Variable	Value (n=252) (%)
Age, mean [range] (years)	68 [23–84]
Sex	
Male	122 [48]
Female	130 [52]
cTNM stage	
Stage IA	186 [74]
Stage IB	66 [26]
Lymphatic invasion	
Positive	83 [33]
Negative	169 [67]
Blood vessel invasion	
Positive	81 [32]
Negative	171 [68]
Pleural invasion	
Positive	48 [19]
Negative	204 [81]
Lymph node metastasis	
Positive	34 [13]
Negative	218 [87]
Histology	
Adenocarcinoma	221 [88]
Non-adenocarcinoma	31 [12]
Whole tumor size, range (mean ± SD) (cm)	0.50–4.00 (2.23±0.75)
Solid-part size, range (mean ± SD) (cm)	0–3.91 (1.67±0.99)
Whole tumor volume, range (mean ± SD) (mm ³)	51–24,393 (4,239±3,975)
Solid-part volume, range (mean ± SD) (mm ³)	0.4–16,344 (2,350±2,761)

TNM, pathological tumor, node and metastasis; SD, standard deviation.

(74%) with stage IA and 66 patients (26%) with stage IB. The mean whole tumor size, solid-part size, whole tumor volume, and solid-part volume were 2.23±0.75 cm, 1.67±0.99 cm, 4,239±3,975 mm³, and 2,350±2,761 mm³ while the median whole tumor size, solid-part size, whole

**Figure 2** Correlation between solid-part size and solid-part volume as determined using Pearson correlation coefficient ($R^2 = 0.59$).

tumor volume, and solid-part volume were 2.18 cm, 1.56 cm, 3,063 mm³ and 1,275 mm³, respectively. The pathological findings indicated that the numbers of patients with Ly, V, PL, and lymph node metastasis were 83 (33%), 81 (32%), 48 (19%), and 34 (13%), respectively.

We analyzed the correlation between solid-part size and solid-part volume using Pearson correlation coefficient ($R^2 = 0.59$; *Figure 2*), and this coefficient value showed a strong correlation. Interobserver agreements for volumetric measurement of a tumor by the dedicated software (ICC =0.977) was higher than the measurement of solid-tumor size on HRCT (ICC =0.925, *Table 2*).

To investigate the impact of HRCT and 3D volumetric parameters for prognostic outcomes, we analyzed the ROC curves for recurrences (*Figure 3*). AUC and the optimal cut-off value relevant to recurrence for whole tumor size, solid-part size, whole tumor volume, and solid-part volume were 0.667 and 2.48 cm (*Figure 3A*), 0.727 and 2.03 cm (*Figure 3B*), 0.654 and 3,258 mm³ (*Figure 3C*), and 0.751 and 1,889 mm³ (*Figure 3D*), respectively. Univariate and multivariate analyses were performed to examine the association between OS or DFS and clinical factors including HRCT and 3D volumetric radiologic features (*Tables 3,4*). Univariate analysis identified the following as significant predictors of unfavorable OS: age ($P=0.032$), male ($P=0.019$), the presence of smoking history ($P=0.037$), whole tumor volume >3,258 mm³ ($P=0.044$), and solid-part volume >1,889 mm³ ($P=0.008$). Multivariate analysis

Table 2 Analysis of interobserver reproducibility of solid-tumor size and solid-tumor volume

Parameter	Patients, n	ICC (95% CI)	P value
Solid-tumor size on HRCT	100	0.925 (0.881–0.956)	<0.001
Solid-tumor volume by volumetric measurement with 3D-VRT	100	0.977 (0.959–0.987)	<0.001

ICC, intra-class correlation coefficient; CI, confidence interval; HRCT, high-resolution computed tomography; 3D-VRT, three-dimensional volume rendered imaging techniques.

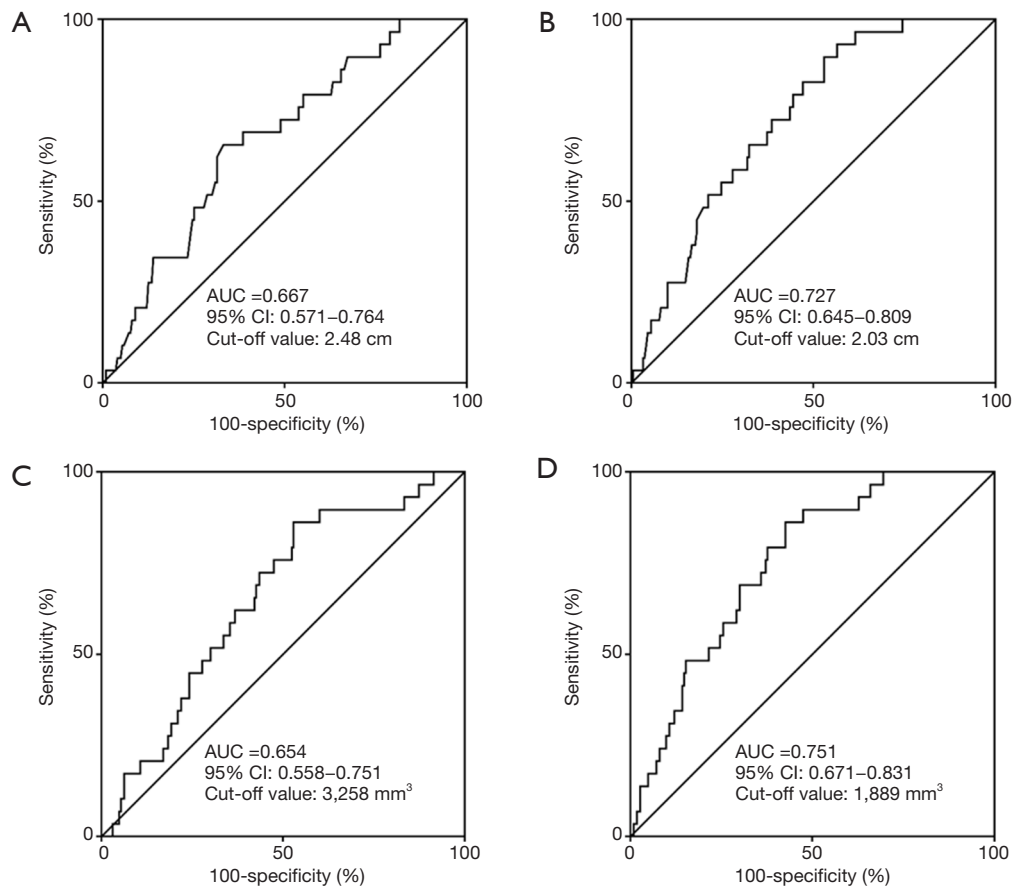


Figure 3 The area under the receiver operating characteristic (ROC) curve for recurrence as determined using whole tumor size (A), soli-part size (B), whole tumor volume (C), and solid-part volume (D) in patients with stage I non-small cell lung cancer patients. AUC, area under the curve; CI, confidence interval.

revealed the following as independently associated with OS (*Table 3*): sex ($P=0.041$) and solid-part volume $>1,889 \text{ mm}^3$ ($P=0.016$). Univariate analysis identified the following as significant predictors of unfavorable DFS: sex ($P=0.001$), the presence of smoking history ($P=0.001$), the serum carcinoembryonic antigen (CEA) value ($P=0.001$), stage IB ($P=0.027$), whole tumor size $>2.48 \text{ cm}$ ($P=0.001$), solid-part size $>2.03 \text{ cm}$ ($P<0.001$), whole tumor volume

$>3,258 \text{ mm}^3$ ($P=0.005$), and solid-part volume $>1,889 \text{ mm}^3$ ($P<0.001$). Multivariate analysis revealed the following as independently associated with DFS (*Table 4*): sex ($P=0.003$), the serum CEA level ($P=0.041$), and solid-part volume $>1,889 \text{ mm}^3$ ($P=0.001$).

We further assessed whether the integrated use of both solid-part size and solid-part volume was beneficial for the prediction of postoperative prognosis. Patients were

Table 3 Univariate and multivariate analyses for overall survival

Variable	Univariate analysis		Multivariate analysis	
	Hazard ratio (95% CI)	P value	Hazard ratio (95% CI)	P value
Age	1.083 (1.007–1.166)	0.032	–	–
Sex (male vs. female)	6.060 (1.340–27.027)	0.019	4.852 (1.069–22.016)	0.041
Smoking history (yes vs. no)	4.953 (1.098–22.349)	0.037	–	–
CEA	1.055 (0.959–1.160)	0.272	–	–
cTNM stage (IB vs. IA)	1.255 (0.386–4.079)	0.705	–	–
Whole tumor size (>2.48 vs. ≤2.48 cm)	2.730 (0.893–8.347)	0.078	–	–
Solid-part size (>2.03 vs. ≤2.03 cm)	2.907 (0.951–8.889)	0.061	–	–
Whole tumor volume (>3,258 vs. ≤3,258 mm ³)	3.756 (1.033–13.548)	0.044	–	–
Solid-part volume (>1,889 vs. ≤1,889 mm ³)	7.733 (1.714–34.889)	0.008	6.452 (1.420–71.190)	0.016

Table 4 Univariate and multivariate analyses for disease-free survival

Variable	Univariate analysis		Multivariate analysis	
	Hazard ratio (95% CI)	P value	Hazard ratio (95% CI)	P value
Age	1.030 (0.990–1.071)	0.141	–	–
Sex (male vs. female)	4.632 (1.893–11.332)	0.001	3.965 (1.614–9.740)	0.003
Smoking history (yes vs. no)	4.739 (1.815–12.346)	0.001	–	–
CEA	1.094 (1.040–1.150)	0.001	1.064 (1.002–1.129)	0.041
cTNM stage (IB vs. IA)	2.237 (1.086–4.608)	0.027	–	–
Whole tumor size (>2.48 vs. ≤2.48 cm)	3.571 (1.669–7.634)	0.001	–	–
Solid-part size (>2.03 vs. ≤2.03 cm)	3.861 (1.805–8.264)	<0.001	–	–
Whole tumor volume (>3,258 vs. ≤3,258 mm ³)	3.226 (1.435–7.246)	0.005	–	–
Solid-part volume (>1,889 vs. ≤1,889 mm ³)	5.952 (2.433–14.493)	<0.001	4.464 (1.783–11.236)	0.001

CI, confidence interval; CEA, carcinoembryonic antigen; TNM, pathological tumor, node and metastasis.

divided into three groups; group A, patients with solid-part size ≤2.03 cm and solid-part volume ≤1,889 mm³; group B, patients with either solid-part size >2.03 cm or solid-part volume >1,889 mm³; group C, patients with solid-part size >2.03 cm and solid-part volume >1,889 mm³. The predictive performance of the pathological invasive factors, and OS and DFS outcomes by using the cut-off values were demonstrated in *Table 5*. Both solid-part size (P<0.001) and solid-part volume (P<0.001) showed a significant correlation with the incidence of pathological invasive factors. Group C also exhibited high proportion of invasive factors compared to Group A (P<0.001). The Kaplan-Meier curves for OS and DFS (*Figure 4*) showed that solid-part size influenced

OS (P=0.050; *Figure 4A*) and DFS (P<0.001; *Figure 4D*) whereas solid-part volume was also significantly correlated with OS (P=0.002; *Figure 4B*) and DFS (P<0.001; *Figure 4E*). Subgroup analysis with the combination revealed that the 4-year OSs of 96.6%, 91.2%, and 87.4% and the 4-year DFSs of 93.4%, 88.4%, and 73.4% for group A, B, and C, respectively (*Figure 4C,F* and *Table 5*). The differences in OS were statistically significant between group A and C (P=0.005), and between group A and B (P=0.018). The differences in DFS between group A and C was statistically significant (P<0.001) while that between group A and B was marginally significant (P=0.093). Together, group C had the most unfavorable OS and DFS compared to group A, B as

Table 5 Prognostic impact of preoperative computed tomographic imaging factors

Variable (n=252)	Invasive factor (negative/positive)		4-year OS		4-year DFS	
	N [%]	P value	%	P value	%	P value
Solid-part size, cm		<0.001		0.050		<0.001
≤2.03	111 [69]/50 [31]		95.2		93.6	
>2.03	30 [33]/61 [67]		88.7		76.1	
Solid-part volume, mm ³		<0.001		0.002		<0.001
≤1,889	104 [72]/41 [28]		96.8		93.8	
>1,889	37 [35]/70 [65]		87.4		75.9	
Integrated use of solid-part size and volume		A vs. B: P<0.001; A vs. C: P<0.001; B vs. C: P=0.536		A vs. B: P=0.018; A vs. C: P=0.005; B vs. C: P=0.845		A vs. B: P=0.093; A vs. C: P<0.001; B vs. C: P=0.129
A	100 [75]/34 [25]		96.6		93.4	
B	15 [39]/23 [61]		91.2		88.4	
C	26 [33]/54 [67]		87.4		73.4	

Invasive factor: positive lymphatic invasion, vascular invasion, pleural invasion, or lymph node metastasis. OS, overall survival; DFS, disease-free survival; A, patients with solid-part size ≤2.03 cm and solid-part volume ≤1,889 mm³; B, patients with either solid-part size >2.03 cm or solid-part volume >1,889 mm³; C, patients with solid-part size >2.03 cm and solid-part volume >1,889 mm³.

well as individual use of either solid-part size or solid-part volume.

Discussion

In this study, we evaluated the survival outcomes and association between CT variables and pathological findings by comparing the predictive performance of whole tumor size, solid-part size, whole tumor volume, and solid-part volume in patients with clinical stage I NSCLC. Multivariate analyses for the prediction of unfavorable OS and DFS showed that solid-part volume had a significant correlation with both outcomes. The combined use of solid-part size and solid-part volume also contributed to the excellent stratification of patients on prognosis.

The ability to preoperatively estimate survival outcomes and the presence of prognostic pathological factors on imaging modalities is crucial to the determination of the appropriate treatment strategy. Lymphatic invasion and blood vessel invasion in patients with NSCLC have been reported to be a strong independent predictor for recurrence (13-16). Preoperative prediction of pathological invasive factors in the current study including lymphatic invasion, blood vessel invasion, pleural invasion, and lymph node metastasis is of importance to select appropriate

surgical procedures since all these factors are responsible for increased recurrence rate and unfavorable prognosis (12-17). A greater number of studies have shown a careful observation of HRCT-based features such as the calculation of consolidation to tumor ratio of lung cancer, and paying attention to the solid-part size of small peripheral lung cancer helps in predicting prognosis and pathological malignancy (2-4,18-20). At present, conducting HRCT before any treatment to evaluate small peripheral NSCLC is mandatory as the maximum diameter of the solid-part serves as a determinant for the latest TNM classification. Although those parameters are very important, it is occasionally difficult to even judge whether the lesion of interest is a predominantly solid or non-solid-predominant tumor because of the irregularity of the solid-part shape.

A 3D virtual lung surgery planning workstation provides surgeons with an effective tool for safe and rational surgery (7-9). In terms of its extensive role, 3D-VRT provides not only visual information for surgical simulations but also quantitative information such as the volume of the lungs and tumor. Takenaka *et al.* reported that the solid-part volume as quantified by the Synapse Vincent system was a prominent predictive factor for DFS compared with the whole tumor volume or solid-part size on HRCT (21). Comparative analysis of interobserver reproducibility of

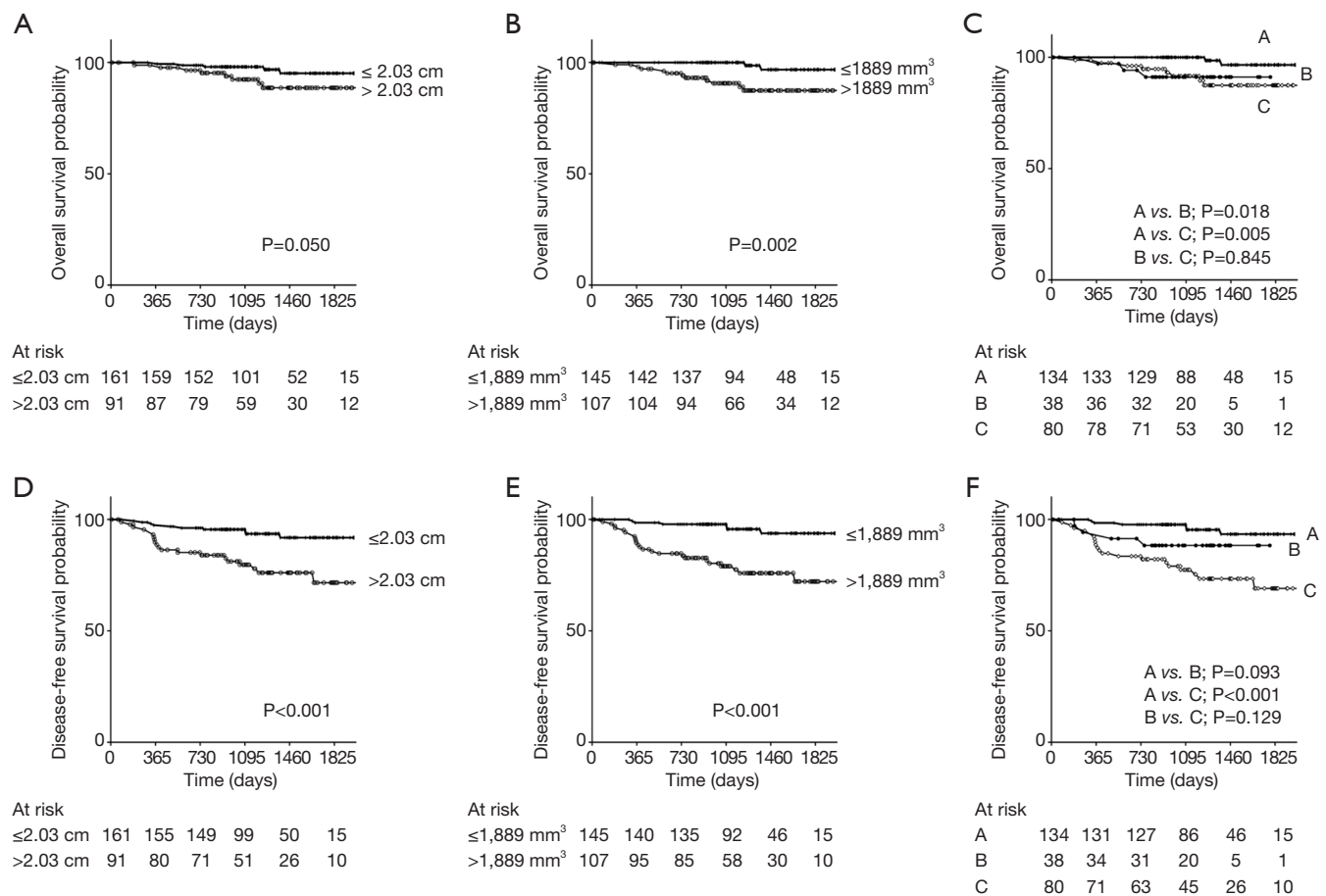


Figure 4 Overall survival (OS) and disease-free survival (DFS) curves of patients with clinical stage I non-small cell lung cancer. All the patients were divided into three groups due to the cut off values of solid-part size and solid-part volume; group A, patients with solid-part size ≤ 2.03 cm and solid-part volume $\leq 1,889$ mm³; group B, patients with either solid-part size > 2.03 cm or solid-part volume $> 1,889$ mm³; group C, patients with solid-part size > 2.03 cm and solid-part volume $> 1,889$ mm³. (A,B) OS curves according to solid-part size (A) and solid-part volume (B) that were dichotomized at each cut-off value, 2.03 cm and 1,889 mm³; (C) OS curves according to the three groups. (D,E,F) DFS curves according to solid-part size (D), solid-part volume (E), and the three groups (F).

solid-tumor size and volume (Table 2) revealed that the workstation semiautomatically provided reproducible and consistent volumetric information of the tumor of interest with ICC of 0.977. Even though the volumetric quantification of a tumor by 3D-VRT is time consuming in contrast to tumor size measurements on conventional axial CT slices, the measurement of solid-part volume for estimating prognostic outcomes such as OS, DFS, and pathological invasive factors supports the successful planning of an appropriate surgical strategy and can contribute to individualized surgical approach including the indication of limited resection for stage I NSCLC. Since there was a strong correlation between solid-part size and

solid-part volume in the current study (Figure 2), solid-part size and solid-part volume resulted in the confounding factors one another. That could be the reason why solid-part size was not independent predictive factors for OS and DFS on our multivariate analyses. The measurement of solid-part size on HRCT is supposed to be fundamental to determine T factor, and simpler and easier method to predict postoperative survival and recurrence. On the contrary, although surgical simulations by 3D-VRT offer us to do better surgical planning and more deeply understand lung cancer pathobiology, this process can be time- and cost-intensive compared with the conducting HRCT alone. Therefore, the proposed application of this data to clinical

scenarios of early-staged lung cancer unless 3D-VRT can be performed routinely would be to add volumetric quantification of lung tumor for a tailored surgical approach when the shape of the solid-part in greatest dimension on HRCT is too irregular and heterogenous to measure in consensus.

The limitations of this study are its retrospective nature and potential bias. The cut-off values of the ROC curves that dichotomized the two groups could be an arbitrarily value and not available universally. We measured tumor volume by initially connecting the end-to-end dimensions of a tumor with a straight line in an axial plane on the workstation, which was similar to the methodology on HRCT. However, once we delineate the end-to-end line, whole tumor volume, solid-part volume, and non-solid-part volume were separately generated semiautomatically with excellent interobserver agreement.

In conclusion, solid-part volume was significantly associated with the prediction of OS, DFS, and the presence of pathological invasive factors. The measurement of not only solid-part size but also solid-part volume is useful in patients with clinical stage I NSCLC when the measurement of the solid-part on HRCT is too complicated due to the chance of inconsistent or irregular-shaped findings.

Acknowledgements

The authors are indebted to the medical editors of the Department of International Medical Communications of Tokyo Medical University for editing the English manuscript. We also thank Ms. Mami Murakami for helping with the statistical analyses of this work.

Footnote

Conflicts of Interest: The authors have no conflicts of interest to declare.

Ethics Statement: This study was approved by the Institutional Ethics Board of Tokyo Medical University (No. 3907).

References

1. Takamochi K, Nagai K, Yoshida J, et al. The role of computed tomographic scanning in diagnosing mediastinal node involvement in non-small cell lung cancer. *J Thorac Cardiovasc Surg* 2000;119:1135-40.
2. Tsutani Y, Miyata Y, Nakayama H, et al. Prognostic significance of using solid versus whole tumor size on high-resolution computed tomography for predicting pathologic malignant grade of tumors in clinical stage IA lung adenocarcinoma: a multicenter study. *J Thorac Cardiovasc Surg* 2012;143:607-12.
3. Asamura H. Minimally invasive approach to early, peripheral adenocarcinoma with ground-glass opacity appearance. *Ann Thorac Surg* 2008;85:S701-4.
4. Suzuki K, Koike T, Asakawa T, et al. A prospective radiological study of thin-section computed tomography to predict pathological noninvasiveness in peripheral clinical IA lung cancer (Japan Clinical Oncology Group 0201). *J Thorac Oncol* 2011;6:751-6.
5. Hattori A, Takamochi K, Matsunaga T, et al. Oncological outcomes of sublobar resection for clinical-stage IA high-risk non-small cell lung cancer patients with a radiologically solid appearance on computed tomography. *Gen Thorac Cardiovasc Surg* 2016;64:18-24.
6. Tsurugai Y, Kozuka T, Ishizuka N, et al. Relationship between the consolidation to maximum tumor diameter ratio and outcomes following stereotactic body radiotherapy for stage I non-small-cell lung cancer. *Lung Cancer* 2016;92:47-52.
7. Ikeda N, Yoshimura A, Hagiwara M, et al. Three dimensional computed tomography lung modeling is useful in simulation and navigation of lung cancer surgery. *Ann Thorac Cardiovasc Surg* 2013;19:1-5.
8. Hagiwara M, Shimada Y, Kato Y, et al. High-quality 3-dimensional image simulation for pulmonary lobectomy and segmentectomy: results of preoperative assessment of pulmonary vessels and short-term surgical outcomes in consecutive patients undergoing video-assisted thoracic surgery. *Eur J Cardiothorac Surg* 2014;46:e120-6.
9. Saji H, Inoue T, Kato Y, et al. Virtual segmentectomy based on high-quality three-dimensional lung modelling from computed tomography images. *Interact Cardiovasc Thorac Surg* 2013;17:227-32.
10. Furumoto H, Shimada Y, Imai K, et al. Prognostic impact of the integration of volumetric quantification of the solid part of the tumor on 3DCT and FDG-PET imaging in clinical stage IA adenocarcinoma of the lung. *Lung Cancer* 2018;121:91-6.
11. Makino Y, Shimada Y, Hagiwara M, et al. Assessment of emphysema severity as measured on three-dimensional computed tomography images for predicting respiratory complications after lung surgery. *Eur J Cardiothorac Surg*

- 2018;54:671-6.
12. Goldstraw P, Chansky K, Crowley J, et al. The IASLC Lung Cancer Staging Project: Proposals for Revision of the TNM Stage Groupings in the Forthcoming (Eighth) Edition of the TNM Classification for Lung Cancer. *J Thorac Oncol* 2016;11:39-51.
 13. Maeda R, Yoshida J, Ishii G, et al. Prognostic impact of intratumoral vascular invasion in non-small cell lung cancer patients. *Thorax* 2010;65:1092-8.
 14. Shimada Y, Saji H, Yoshida K, et al. Pathological vascular invasion and tumor differentiation predict cancer recurrence in stage IA non-small-cell lung cancer after complete surgical resection. *J Thorac Oncol* 2012;7:1263-70.
 15. Mimae T, Tsutani Y, Miyata Y, et al. Role of lymphatic invasion in the prognosis of patients with clinical node-negative and pathologic node-positive lung adenocarcinoma. *J Thorac Cardiovasc Surg* 2014;147:1820-6.
 16. Neri S, Yoshida J, Ishii G, et al. Prognostic impact of microscopic vessel invasion and visceral pleural invasion in non-small cell lung cancer: a retrospective analysis of 2657 patients. *Ann Surg* 2014;260:383-8.
 17. Kawase A, Yoshida J, Miyaoka E, et al. Visceral pleural invasion classification in non-small-cell lung cancer in the 7th edition of the tumor, node, metastasis classification for lung cancer: validation analysis based on a large-scale nationwide database. *J Thorac Oncol* 2013;8:606-11.
 18. Okada M, Nishio W, Sakamoto T, et al. Discrepancy of computed tomographic image between lung and mediastinal windows as a prognostic implication in small lung adenocarcinoma. *Ann Thorac Surg* 2003;76:1828-32; discussion 1832.
 19. Uehara H, Tsutani Y, Okumura S, et al. Prognostic role of positron emission tomography and high-resolution computed tomography in clinical stage IA lung adenocarcinoma. *Ann Thorac Surg* 2013;96:1958-65.
 20. Matsuguma H, Yokoi K, Anraku M, et al. Proportion of ground-glass opacity on high-resolution computed tomography in clinical T1 N0 M0 adenocarcinoma of the lung: A predictor of lymph node metastasis. *J Thorac Cardiovasc Surg* 2002;124:278-84.
 21. Takenaka T, Yamazaki K, Miura N, et al. The Prognostic Impact of Tumor Volume in Patients with Clinical Stage IA Non-Small Cell Lung Cancer. *J Thorac Oncol* 2016;11:1074-80.

Cite this article as: Shimada Y, Furumoto H, Imai K, Masuno R, Matsubayashi J, Kajiwara N, Ohira T, Ikeda N. Prognostic value of tumor solid-part size and solid-part volume in patients with clinical stage I non-small cell lung cancer. *J Thorac Dis* 2018;10(12):6491-6500. doi: 10.21037/jtd.2018.11.08